Anton Bergant, Arris S. Tijsseling, John P. Vítkovský, Dídia I. C. Covas, Angus R. Simpson and Martin F. Lambert

Parameters affecting water-hammer wave attenuation, shape and timing. Part 2: Case studies

Journal of Hydraulic Research, 2008; 46(3):382-391

Parameters affecting water hammer wave attenuation, shape and timing. Part 2: Case studies

by

Bergant, A., Tijsseling, A., Vítkovský, J.P., Covas, D., Simpson, A.R. and Lambert, M.F.

Journal of Hydraulic Research

Citation:
Bergant, A., Tijsseling, A., Vítkovský, J.P., Covas, D., Simpson, A.R. and Lambert, M.F. (2008). "Parameters affecting water hammer wave attenuation, shape and timing. Part 2: Case studies", *Journal of Hydraulic Research,* IAHR, Vol. 46, No. 3, 382–391

Parameters affecting water-hammer wave attenuation, shape and timing - Part 2: Case studies

Paramètres affectant l'atténuation, la forme et le retard du coup de bélier - Partie 2: Cas d'étude

ANTON BERGANT, *Litostroj E.I. d.o.o, 1000 Ljubljana, Slovenia (author for correspondence)*

ARRIS S TIJSSELING, *Eindhoven University of Technology, P.O. Box 513, 5600 MB Eindhoven, The Netherlands*

JOHN P VÍTKOVSKÝ, *Department of Natural Resources and Water, Indooroopilly QLD 4068, Australia*

DÍDIA COVAS, *Instituto Superior Técnico, 1049-001 Lisboa, Portugal*

ANGUS R SIMPSON, *The University of Adelaide, Adelaide SA 5005, Australia*

MARTIN F LAMBERT, *The University of Adelaide, Adelaide SA 5005, Australia*

ABSTRACT

This twin paper investigates parameters that may significantly affect water-hammer wave attenuation, shape and timing. Possible sources that may affect the waveform predicted by classical water hammer-theory include unsteady friction, cavitation (including column separation and trapped air pockets), a number of fluid-structure interaction (FSI) effects, viscoelastic behaviour of the pipe-wall material, leakages and blockages. Part 1 of the twin paper presents the mathematical tools needed to model these sources. Part 2 of the paper presents a number of case studies showing how these modelled sources affect pressure traces in a simple reservoir-pipeline-valve system. Each case study compares the obtained results with the standard (classical) water-hammer model, from which conclusions are drawn concerning the transient behaviour of real systems.

RÉSUMÉ

Cet article, publié en deux parties, étudie les paramètres qui peuvent avoir un effet significatif sur l'atténuation, la forme et le retard de la variation de pression pendant un coup de bélier. Les phénomènes non considérés par la théorie classique du coup de bélier qui peuvent modifier la forme d'onde sont notamment la friction transitoire, la cavitation (y compris la séparation de la

colonne et les poches d'air), l'interaction entre le fluide et la structure (FSI), le comportement viscoélastique du matériel de la conduite, les fuites et les blocages. La première partie de cet article présente les modèles mathématiques de calcul des effets de ces phénomènes. La deuxième partie présente une étude de cas qui illustre l'effet de ces phénomènes sur la variation de pression dans un système simple, composé d'un réservoir, d'une conduite et d'une valve. Dans l'étude de cas, les résultats obtenus sont comparés avec ceux du modèle classique du coup de bélier. Les conclusions sur le comportement réel des systèmes de conduites pendant le régime transitoire du coup de bélier sont tirées à partir de ces résultats.

Keywords: Water hammer, unsteady friction, cavitation, column separation, air pocket, fluid-structure interaction, viscoelastic behaviour of the pipe-wall, leakage, blockage.

1 Introduction

A number of numerical case studies are presented to show how the effects of unsteady friction, cavitation (including column separation and trapped air pockets), fluid-structure interaction, viscoelastic behaviour of the pipe-wall, leakage and blockage change the water-hammer waveform predicted by classical theory. All these phenomena can be important and explain certain observations in field and laboratory. However, to identify these phenomena it is desirable to study their effects in the very same piping system. A simple reservoir-pipeline-valve system has been selected for clarity. The system is simulated using a standard water-hammer model based on Eqs. (1) and (2) in Part 1 of the twin paper, and a corresponding method of characteristics (MOC) numerical model that incorporates unsteady friction (for laminar and turbulent flow), cavitation (vaporous and gaseous), fluid-structure interaction (Poisson and junction coupling), viscoelastic behaviour of the pipe wall, leakage and blockage, or a combination of these, as described in Part 1. The objective of this paper is not to validate once again proven models, but to show and compare the effects of the different phenomena in a clear and simple way. The used models have been previously verified with measurements in a number of research publications:

(1) Unsteady friction model (Bergant *et al*. 2001; Vítkovský 2001; Bergant *et al*. 2003; Vítkovský *et al*. 2006),
(2) Cavitation model (Wylie and Streeter 1993; Bergant and Simpson 1999; Bergant and Tijsseling 2001),

(3) Fluid-structure interaction model (Tijsseling *et al.* 1996; Vardy *et al.* 1996),
(4) Pipe wall viscoelastic model (Bergant *et al*. 2003; Covas *et al*. 2004, 2005),
(5) Leakage and blockage model (Vítkovský 2001; Wang 2002).

The standard water-hammer model is herein referred to as the 'classical model'.

1.1 Test pipeline system

The test system used for investigating water-hammer waveforms comprises a straight L = 37.2 m long sloping copper pipeline of D = 22 mm internal diameter and e = 1.6 mm wall thickness connecting two tanks (Fig. 1). For the numerical investigation of viscoelastic behaviour of the pipe-wall a medium-density polyethylene pipeline of the same dimensions is used instead of the copper pipeline. The pipe-wall is assumed to be hydraulically smooth. The test apparatus is equivalent to the experimental apparatus that is installed in the Robin Hydraulic Laboratory in the School of Civil and Environmental Engineering at the University of Adelaide (Bergant *et al.* 2001).

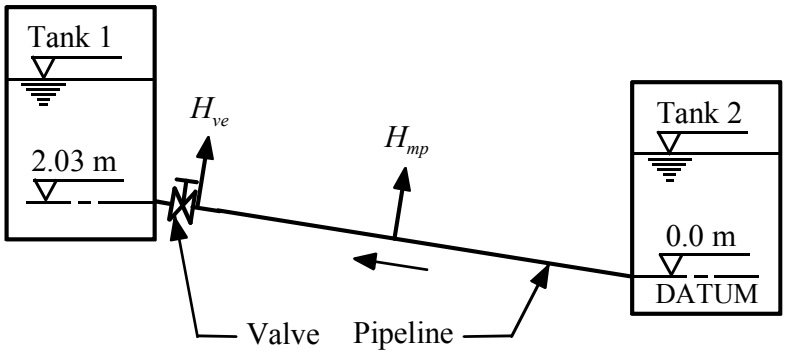

Figure 1 Test pipeline system (length L = 37.2 m; internal diameter D = 22 mm).

The transient event is generated by the rapid closure of a downstream ball-type valve. The initial discharge in the case studies is $Q_0 = 0.076 \times 10^{-3}$ m^3/s (initial Reynolds number $\mathbf{Re}_0$ = 4,360) and the static head in tank 2 is H_{T2} = 32 m (pressure head difference between the two tanks is $\Delta h_{T2\rightarrow T1,0}$ = 0.14 m); however, to obtain liquid column separation, $Q_0 = 0.114 \times 10^{-3}$ m^3/s ($\mathbf{Re}_0$ = 6,540) and H_{T2} = 22 m ($\Delta h_{T2\rightarrow T1,0}$ = 0.26 m). The valve closure time for all cases is t_c = 0.009 s. The liquid wave speed a is 1319 m/s in the copper pipe and 231 m/s in the medium-density polyethylene pipe. The number of reaches in all numerical simulations is N = 32.

2 Unsteady friction

Traditionally the steady pipe flow friction approximation is incorporated in commercial water-hammer software packages. This assumption is satisfactorily applied to slow transients where the wall shear stress has a quasi-steady behaviour. Experimental validation of the steady friction model for rapid transients has shown significant deficiencies in attenuation, shape and timing of pressure waves (Bergant *et al*. 2001). The effect of unsteady friction on water-hammer waveforms is investigated using the copper pipeline shown in Fig. 1. Numerical results from the 'classical model' (steady friction) and the unsteady friction model (pure convolution-based model of Zielke (1968)) are compared. The Reynolds number of the initial flow ($\mathbf{Re}_0$) is 4,360 so that the initial flow is turbulent. The smooth-pipe turbulent Vardy-Brown weighting function (W_{app}) formulae are used (Vardy and Brown 2003) - Fig. 2.

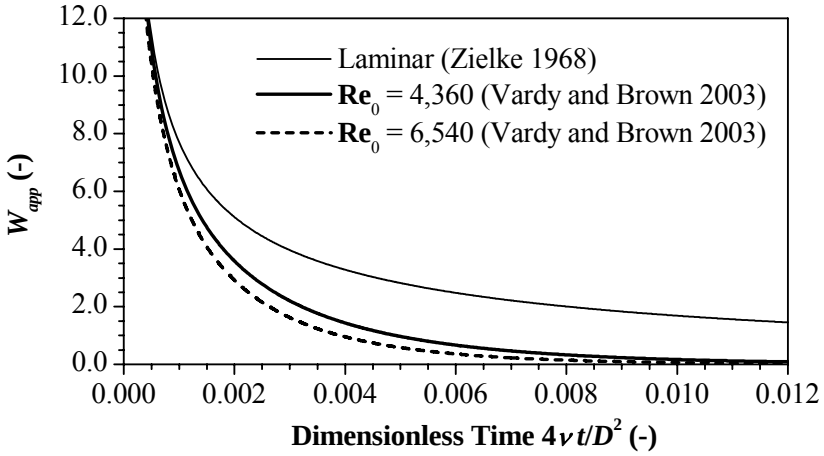

Figure 2 Weighting functions (W_{app}) for transient laminar flow (Zielke 1968) and smooth-pipe turbulent flow (Vardy and Brown 2003).

The results are compared at the valve (H_{ve}) and at the midpoint (H_{mp}) and are presented in Fig. 3. The simulations show that the steady friction approximation in the classical model underestimates the damping and dispersion predicted by the physically more correct unsteady friction model. Additionally, the steady friction model is not able to produce the evolution of the typical shape of the pressure oscillations, demonstrating its inability to model strong frequency-dependent attenuation.

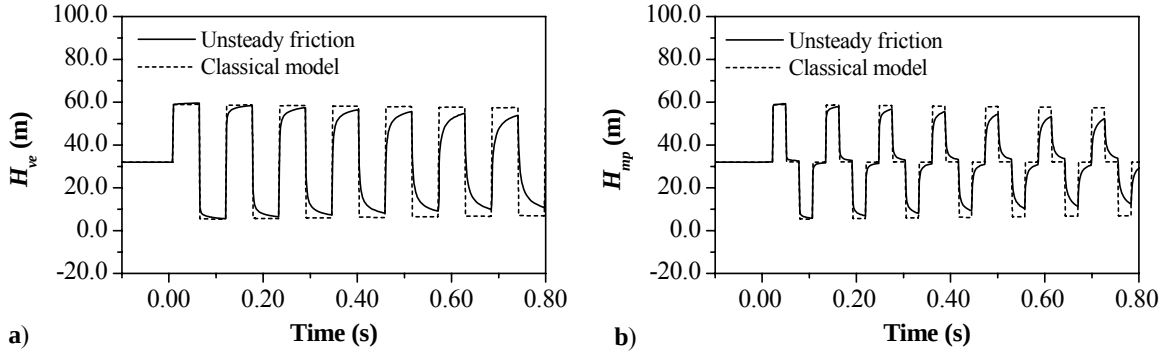

Figure 3 Comparison of heads at the valve (H_{ve}) and at the midpoint (H_{mp}) in a copper pipeline; $\mathbf{Re}_0$ = 4,360.

3 Cavitation

The effect of vaporous and gaseous cavitation on the transient waveform is investigated in the copper pipeline apparatus - see Fig. 1.

3.1 Vaporous cavitation

Computational results are presented for the case with initial discharge $Q_0 = 0.114 \times 10^{-3}$ m^3/s. A weighting factor of $\psi = 1.0$ is used in the discrete vapour cavity model (DVCM) (Simpson and Bergant 1994).

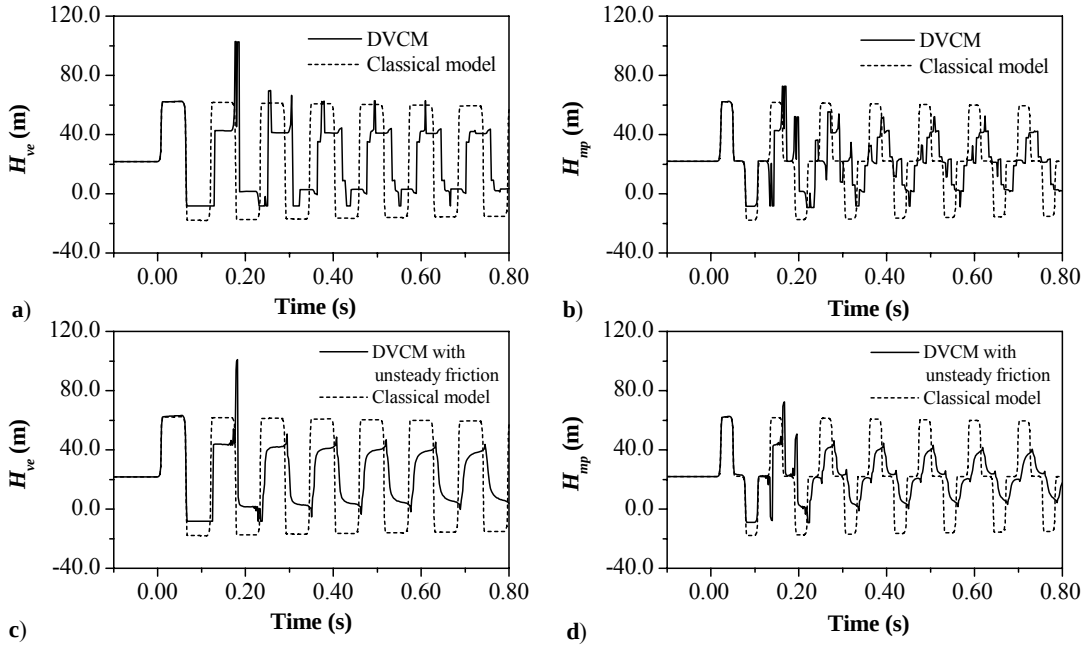

Figure 4 Comparison of heads at the valve (H_{ve}) and at the midpoint (H_{mp}) in a copper pipeline; $\mathbf{Re}_0$ = 6,540.

Computational results from the 'classical model' and the DVCM are compared at the valve (H_{ve}) and at the midpoint (H_{mp}) and are depicted in Fig. 4. The 'classical model' results (Figs. 4(a) and 4(b)) significantly differ from the DVCM (with steady friction) results. The actual flow situation concerns a column separation case with a maximum head significantly larger than the water-hammer head in pure liquid (at the valve - DVCM: $H_{ve,max}$ = 102.7 m; 'classical model': $H_{ve,max}$ = 62.3 m). The minimum pressure head predicted by the 'classical model' is well below the liquid vapour pressure head. The assumption of fluid homogeneity and continuity in the 'classical model' is violated when the pressure drops to the liquid vapour pressure. In this case, the liquid starts to vaporize and a large vapour cavity is formed at the valve. Some time after the first large cavity collapsed, a short-duration peak is super-imposed on the pressure head produced by the first cavity collapse.

A convolution-based unsteady friction model (Zielke 1968) was incorporated into the DVCM to show the combined effects of vaporous cavitation and unsteady friction. The weighting function for the initial flow with a Reynolds number of 6,540 was calculated using the Vardy-Brown weighting function (W_{app}) shown in Fig. 2. The results from the DVCM with unsteady friction are presented in Figs. 4(c) and 4(d). Although the bulk transient response remains the same, the inclusion of unsteady friction generates a significant damping of the pressure spikes.

3.2 Gaseous cavitation

Computational runs were performed using the discrete gas cavity model (DGCM) (Wylie 1984; Wylie and Streeter 1993) for two distinct flow situations:

(1) Gaseous cavitation in liquid with free gas present at all computational sections (simulation of pressure waves in bubbly flow),
(2) Trapped gas pocket at 13.95 m upstream of the valve (at the 3/8th point from the valve).

A weighting factor of $\psi = 1.0$ has been used in the DGCM (Wylie 1984). Six different values of free gas void fraction (ratio of gas volume to total volume) $\alpha_{g0} = \{10^{-7}; 10^{-6}; 10^{-5}; 10^{-4}; 10^{-3}$ and $10^{-2}\}$ at atmospheric conditions were selected in the analysis for both flow situations (initial discharge $Q_0 = 0.076 \times 10^{-3}$ m^3/s). The aim of the analysis was to identify the effect of the amount of free gas on fluid transients. Computational results from the DGCM (with steady friction) are compared with 'classical model' results at the valve (H_{ve}) and at the midpoint (H_{mp}) and are depicted in Figs. 5 and 6, respectively.

3.2.1 Liquid with free gas present at all computational sections

The DGCM results with a very low gas void fraction $\alpha_{g0} = 10^{-7}$ (Figs. 5(a) and 5(b)) perfectly match the 'classical model' results. The DGCM is capable of simulating water-hammer events in nearly 'pure' liquid. The DGCM results with a low gas void fraction $\alpha_{g0} = 10^{-5}$ (Figs. 5(c) and 5(d)) reveal a weak effect of small amounts of free gas. The discrepancies between the DGCM results and the 'classical model' results increase with increasing gas void fraction. Figs. 5(e) and 5(f) display DGCM results with a large gas void fraction $\alpha_{g0} = 10^{-3}$. The actual flow situation represents a gaseous cavitation case with a maximum head significantly smaller than the water-hammer head (at the valve - DGCM: $H_{ve,max} = 52.6$ m; 'classical model': $H_{ve,max} = 58.9$ m).

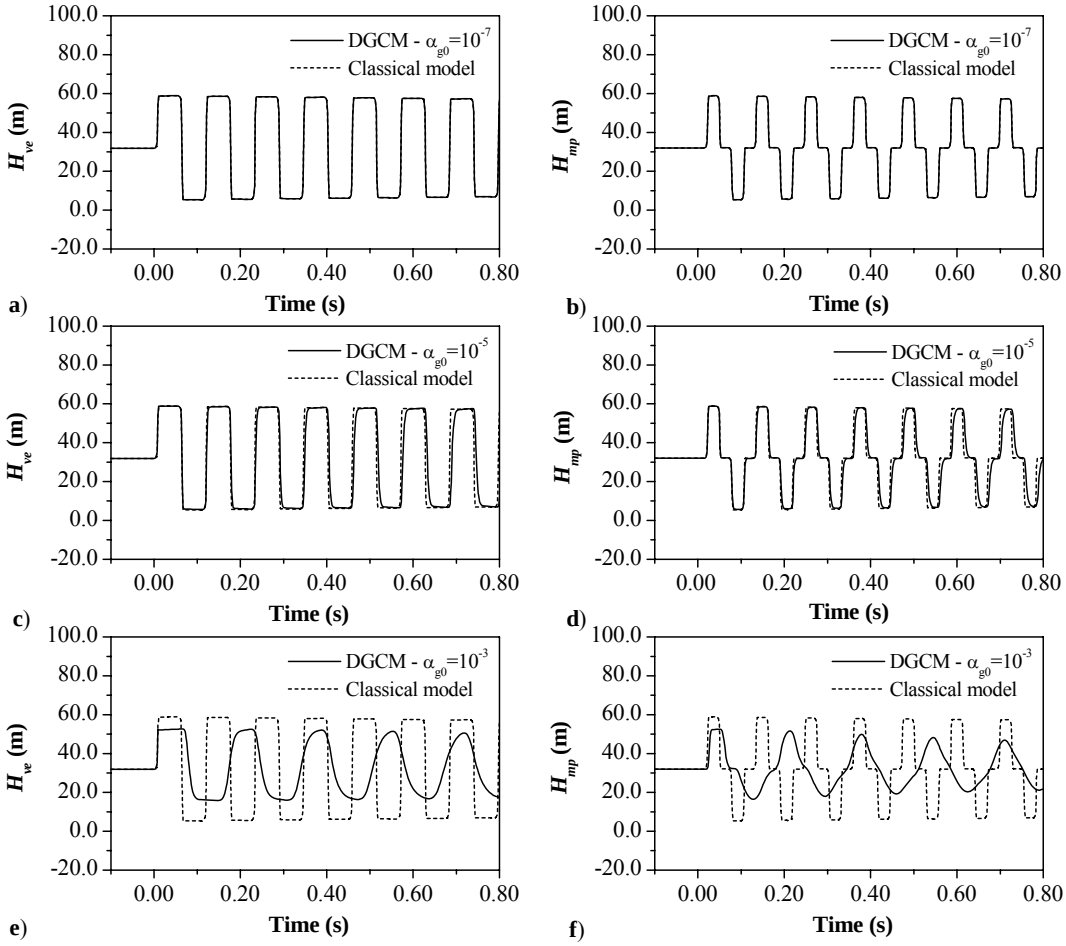

Figure 5 Comparison of heads at the valve (H_{ve}) and at the midpoint (H_{mp}) in a copper pipeline; $\mathbf{Re}_0$ = 4,360.

3.2.2 Trapped gas pocket at the 3/8th point from the valve

In our case study, a single gas pocket is assumed to be trapped 13.95 m upstream of the valve (at the 3/8th point from the valve) in the copper pipeline. Six computational runs with void fractions of the trapped gas pocket $\alpha_{g0,3/8}$ = {10^{-7}; 10^{-6}; 10^{-5}; 10^{-4}; 10^{-3} and 10^{-2}} have been performed. The corresponding gas volume is still small in comparison to the total water volume. The DGCM has been used with a large void fraction at the 3/8th point and much smaller void fractions of 10^{-7} at the other computational sections.

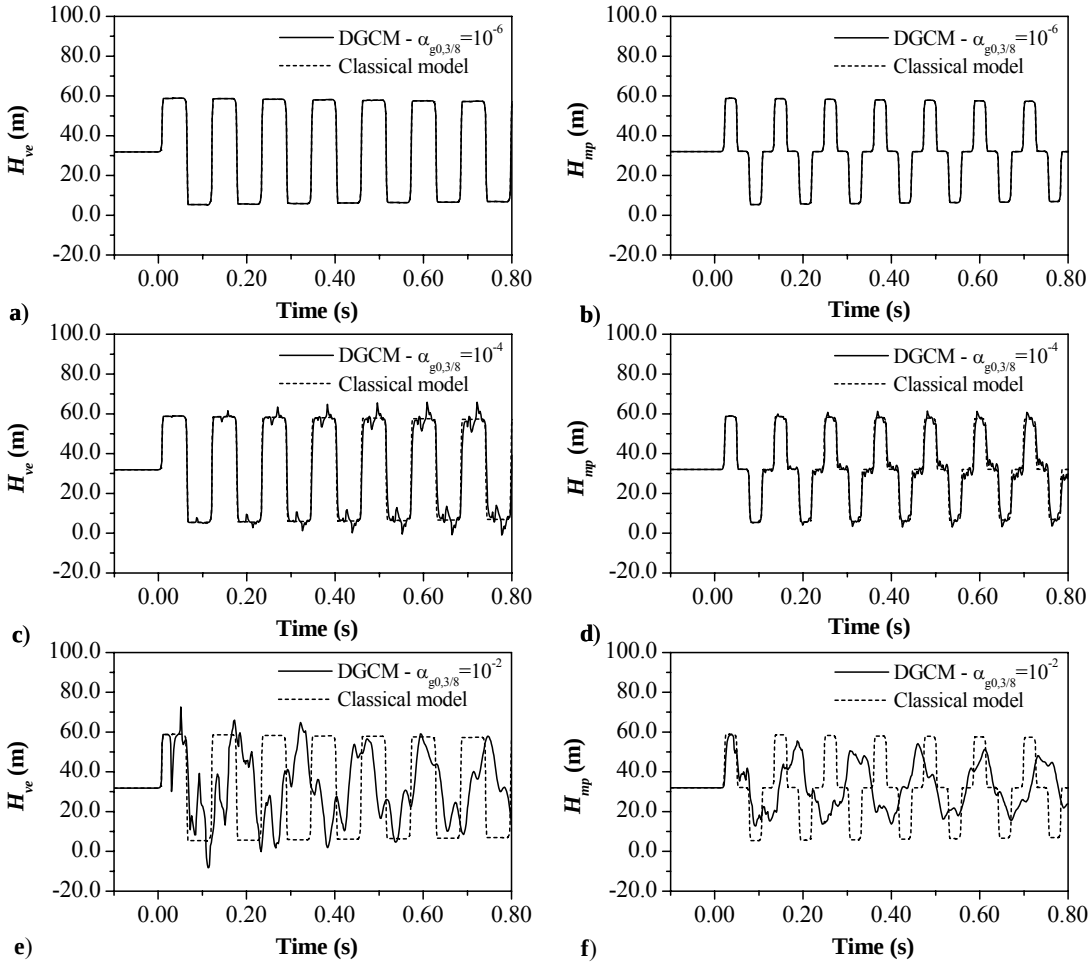

Figure 6 Comparison of heads at the valve (H_{ve}) and at the midpoint (H_{mp}) in a copper pipeline; $\mathbf{Re}_0 = 4{,}360$.

A very small volume of the trapped gas pocket $\alpha_{g0,3/8} = 10^{-6}$ (Figs. 6(a) and 6(b)) does not visibly affect the pressure wave. The DGCM results with a small trapped gas pocket - $\alpha_{g0,3/8} = 10^{-4}$ (Figs. 6(c) and 6(d)) show a weak effect of the trapped pocket on the pressure traces. Longer simulations show that a beat develops. The discrepancies between the DGCM results and the 'classical model' results increase with increasing volume of the trapped gas pocket. Figs. 6(e) and 6(f) present DGCM results with a large gas void fraction - $\alpha_{g0,3/8} = 10^{-2}$. In this case, the actual flow situation represents a gaseous cavitation case with a maximum head larger than the water-hammer head in 'pure' liquid (at the valve - DGCM: $H_{ve,max} = 67.7$ m; 'classical model': $H_{ve,max} = 58.9$ m).

4 Fluid-structure interaction

The test pipeline shown in Fig. 1 is used to theoretically study the possible effects of FSI. Therefore, the 37.2 m long straight copper pipe (E = 120 GPa, ρ_s = 8960 kg/m^3, ν = 0.34) is assumed not to be restrained against axial motion along its entire length. The tank at its upstream end is a fixed point, and the valve downstream (assumed to be of negligible mass) is either fixed or free to move, depending on the type of FSI under investigation. The pressure and axial stress wave speeds are taken as $\tilde{a}$ = 1316.5 m/s and $\tilde{a}_s$ = 3686.2 m/s, so that their ratio is 5/14. A non-staggered computational grid with 5 × 32 = 160 reaches, but with $\Delta t = 5\,\Delta x / \tilde{a}$, allows standard MOC calculation without interpolation (except for the boundary values needed at $\Delta t = \Delta x / \tilde{a}$ intervals) (Tijsseling and Lavooij 1989). The effects of the different FSI mechanisms on the classical water-hammer waveform are demonstrated in the four cases below.

4.1 Poisson coupling

To study solely the effects of Poisson coupling (without friction), the valve is assumed to be fixed (immovable). Valve closure generates a travelling pressure rise, which radially expands the pipe wall. The radial expansion is accompanied with an axial contraction, which sends out a stress wave and an associated pressure change in the fluid (precursor). These effects are initially very small as can be seen from the pressure heads in Figs. 7(a) and 7(b): the first period of water hammer is not much affected by FSI. However, Figs. 7(a) and 7(b) also show that the effects cumulate to such an extent that unrealistically high and low pressures result. There is a continuous exchange and redistribution of energy between the water-hammer wave and the vibrating pipe. A beat phenomenon develops (Tijsseling 1997). Precursor waves have been observed in laboratory experiments, but as far as the authors know, *Poisson-coupling beat* has not (although Fig. 4(a) of Budny *et al.* (1991) and Fig. 16 of Vennatrø (1999) exhibit cumulative Poisson effects). Three obvious reasons are (i) unsteady friction and rubbing at pipe supports damp the transient event, (ii) pipe anchors never are entirely stiff or entirely inert when impact loaded, and (iii) pipes like to vibrate in their lowest and hence flexural mode, which is made possible through axial-lateral coupling at supports.

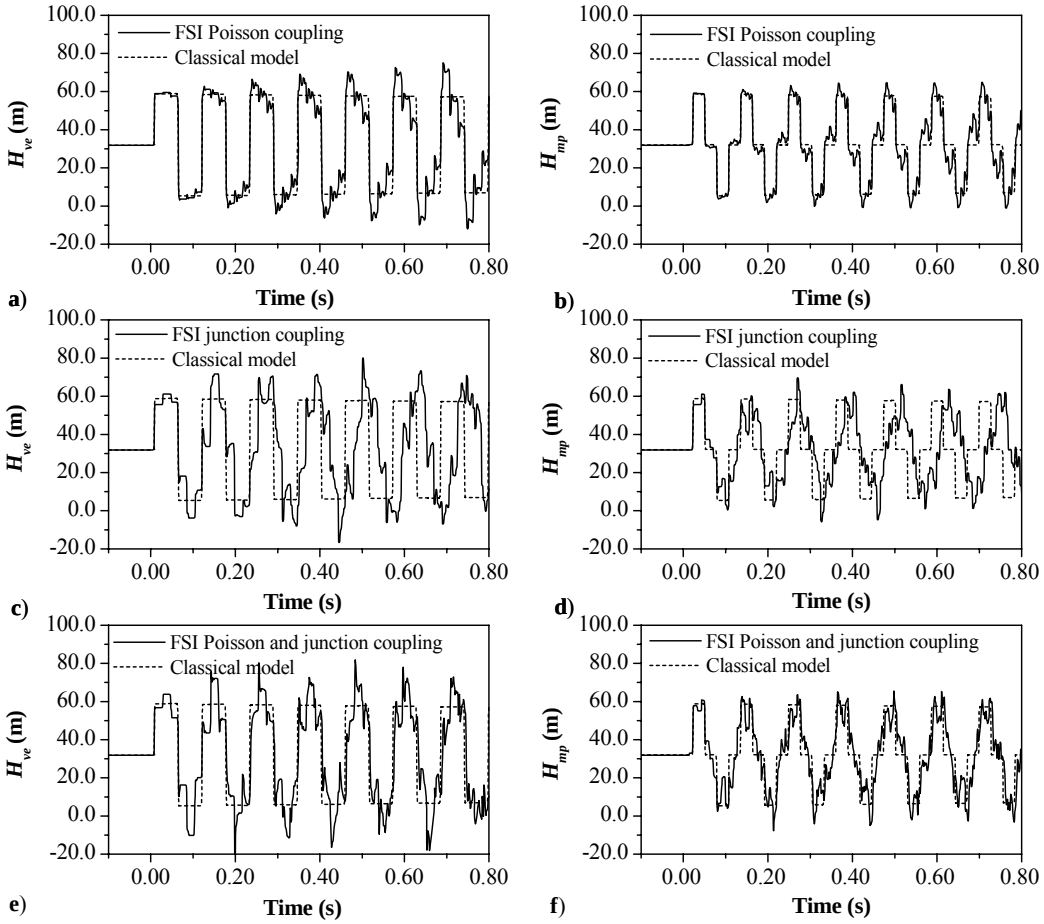

Figure 7 Comparison of heads at the valve (H_{ve}) and at the midpoint (H_{mp}) in a copper pipeline; $\mathbf{Re}_0 = 4{,}360$.

4.2 Junction coupling

To study solely the effects of junction coupling (without friction), Poisson's ratio is set equal to zero so that the mechanisms described in the previous section do not exist. The valve is free to move now; it follows the pipe vibration. The pressure rise generated by valve closure pushes the valve in downstream direction, thereby creating additional storage for the fluid and as a result a lower initial pressure rise, Figs. 7(c) and 7(d). The fluid is not brought entirely to rest; it has the velocity of the valve. The axial stress wave generated by the movement of the valve travels to and from the upstream tank and at its return, after time $2L/\widetilde{a}_s$, it pulls the valve back. This "pumping" action explains the second pressure rise in Figs. 7(c) and 7(d). In contrast to the Poisson-coupling case, Figs. 7(a) and 7(b), junction coupling makes the pressure out of phase with classical water hammer, Figs. 7(c) and 7(d). The system becomes slower than the classical

$4L/a$ system, mainly because $\nu = 0$ and $\alpha = 1$ in the FSI solution, and $\nu = 0.34$ and $\alpha = 0.87$ in the classical solution (see Part 1, Eq. (4)).

4.3 Poisson and junction coupling

Figures 7(e) and 7(f) show the combined effects of Poisson and junction coupling (without friction). Readers with good eyes may be able to spot the precursor wave travelling ahead of the main water-hammer wave in Fig. 7(f). It is evident that FSI, when compared with the classical model, causes larger extreme pressures, high-frequency fluctuations, and a phase shift. It is noted that in multi-pipe systems with unrestrained elbows FSI may also cause, after one water-hammer period, a profound damping of the pressure wave as a consequence of water hammer-induced flexural pipe vibration (Erath *et al*. 1999). FSI will not cause damping in unrestrained single-pipe systems.

4.4 FSI and cavitation

Figure 8 shows the combined effects of Poisson coupling, junction coupling and vaporous cavitation (DVCM with steady friction). A large phase shift and high-frequency fluctuations are the most striking features. The subject of FSI and cavitation has been extensively dealt with in Tijsseling (1993).

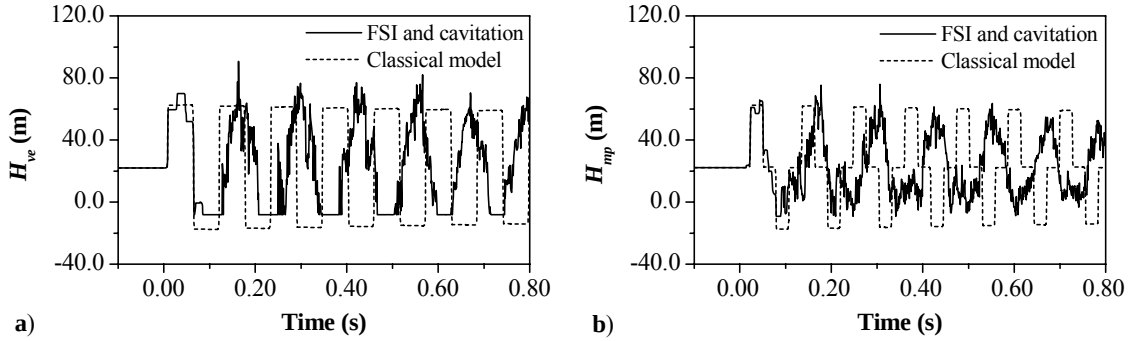

Figure 8 Comparison of heads at the valve (H_{ve}) and at the midpoint (H_{mp}) in a copper pipeline; $\mathbf{Re}_0 = 6{,}540$.

5 Viscoelastic behaviour of the pipe wall

In this theoretical case study, the creep-compliance function taken from Gally *et al*. (1979) is for medium-density polyethylene at a temperature of 25°C and it is described by a three-element Kelvin-Voigt model where J_k = {0.754×10^{-9}, 1.046×10^{-9}, 1.237×10^{-9}} Pa^{-1} and τ_k = {0.89×10^{-4}, 0.0222, 1.864} s^{-1}; k = 1, 2, 3. This creep-compliance function is shown in Fig. 9. The elastic component of the creep-compliance function corresponds to an elastic Young's modulus of E = 0.649 GPa. A constant Poisson's ratio is assumed as ν = 0.5. The parameter α depends on the axial pipe constraints and is estimated to be α = 0.863.

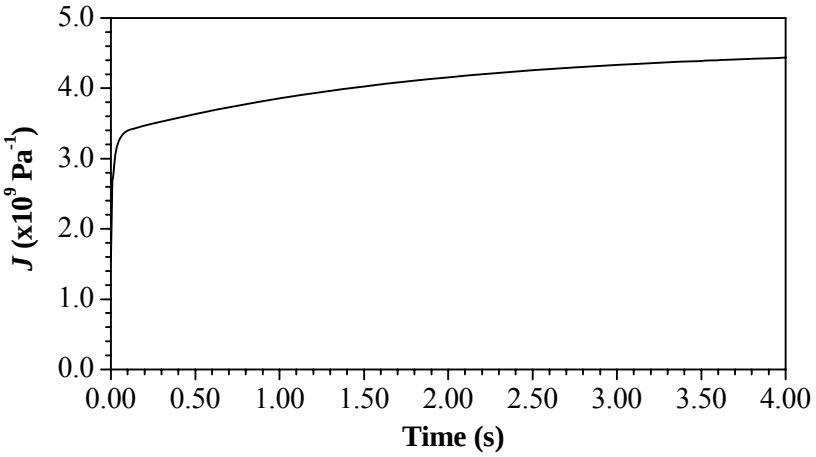

Figure 9 Creep-compliance function (J) for medium-density polyethylene (Gally *et al*. 1979).

Figs. 10(a) and 10(b) show the viscoelastic effect (with steady friction) on the pressure histories at valve and midpoint in the plastic pipeline (Fig. 1). The lower phase velocity, dispersion and higher attenuation are clear from the pressure responses. In addition to the lower initial pressure rise, the small initial peak rapidly attenuates to a plateau. Figs. 10(c) and 10(d) show the comparison of the classical response with the viscoelastic response with unsteady friction. The convolution-type unsteady friction model is used in combination with a smooth-pipe turbulent Vardy-Brown weighting function (W_{app}) for $\mathbf{Re}_0$ = 4,360 (Fig. 2). The numerical results in Figs. 10(c) and 10(d), when compared with the Figs. 10(a) and 10(b), show that the addition of unsteady friction has hardly any effect on the pressure response other than a slightly higher damping and dispersion of the pressure wave. This means that the effect of the viscoelastic behaviour of the pipe wall in the transient event, in this example, is dominant over unsteady friction. This phenomenon has been observed and discussed by Covas *et al*. (2004, 2005).

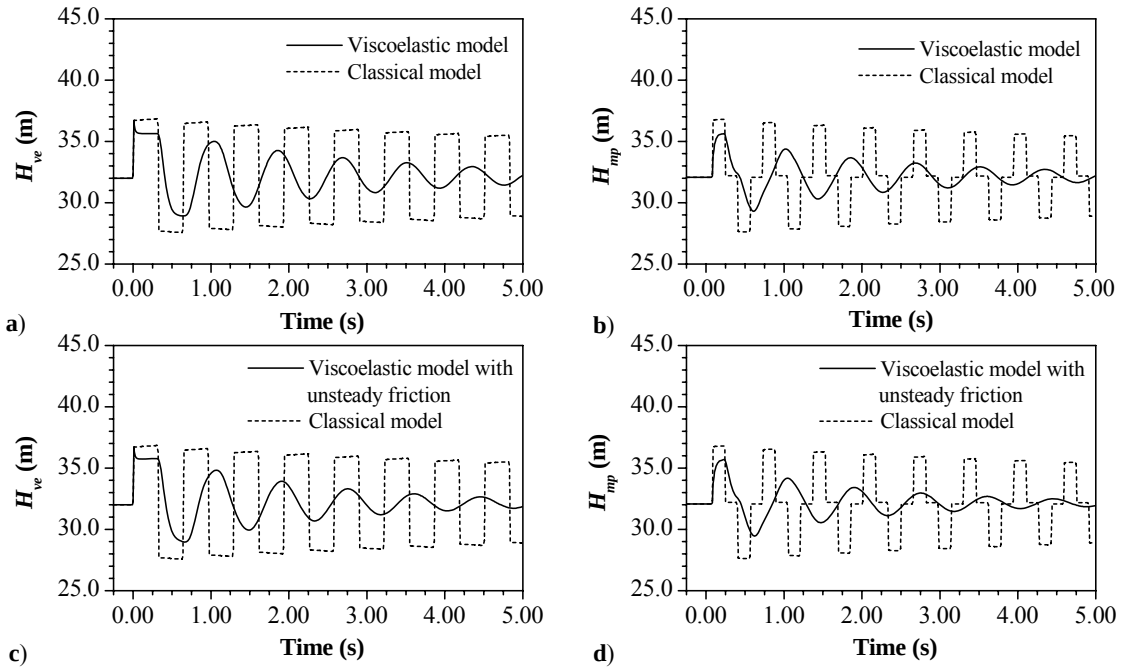

Figure 10 Comparison of heads at the valve (H_{ve}) and at the midpoint (H_{mp}) in a medium-density polyethylene pipeline; $\mathbf{Re}_0 = 4{,}360$.

6 Discrete leakage and blockage

The effect of a leak and a blockage located 13.95 m upstream of the valve (at the 3/8th point from the valve) in the copper pipeline is investigated (Fig. 1). Each pipeline fault was sized such that the steady state ratios of leak flow to pipe flow, and of blockage head to reservoir head, were equal.

6.1 Discrete leakage

The leak has a diameter of 0.52 mm and a weighted area $C_d A_{Or} = 15.25\times10^{-8}$ m^2. This gives a leak area to cross-sectional pipe area ratio of 0.056%. The ratio of the leak flow to the steady-state flow through the pipeline is 5%. Fig. 11 shows the effect of the discrete leak on the pressure response at the valve and at the midpoint using both the steady friction model and the convolution-based unsteady friction model (Vardy and Brown 2003). The presence of a leak increases the damping in the system. Additionally, the pressure response is more complicated due to reflections from the leak. The use of the convolution-based unsteady friction model damps

the leak-induced reflections as the simulation time progresses, which is to be expected in a system where unsteady friction is dominant.

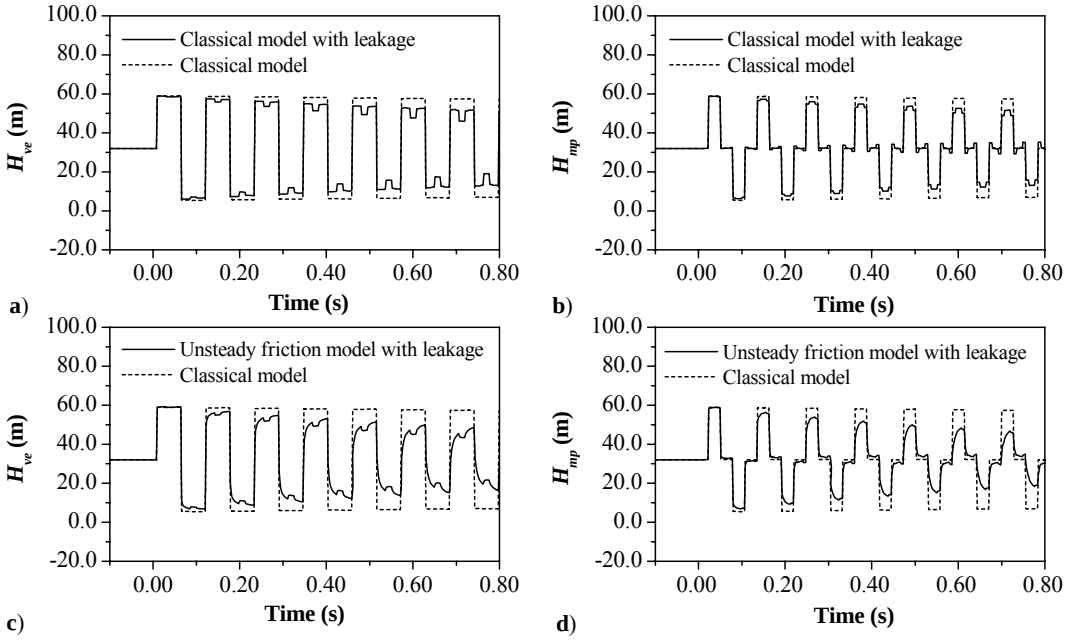

Figure 11 Comparison of heads at the valve (H_{ve}) and at the midpoint (H_{mp}) in a copper pipeline; $\mathbf{Re}_0$ = 4,360.

6.2 Discrete blockage

The blockage has a diameter of 4.94 mm and a weighted area C_dA_{Or} = 1.33×10^{-5} m^2 and it is located at the same position in the pipeline as the leak. This gives a blockage area to pipe area ratio of 5%. The ratio of the head loss across the blockage to the steady-state head in the pipeline is 5% (similar to leak flow). Fig. 12 shows the pressure response for the blocked pipeline. Looking at the shape of the pressure response, the blockage effect is somehow the opposite of the leak effect. The inclusion of the unsteady friction model damps the reflections from the blockage.

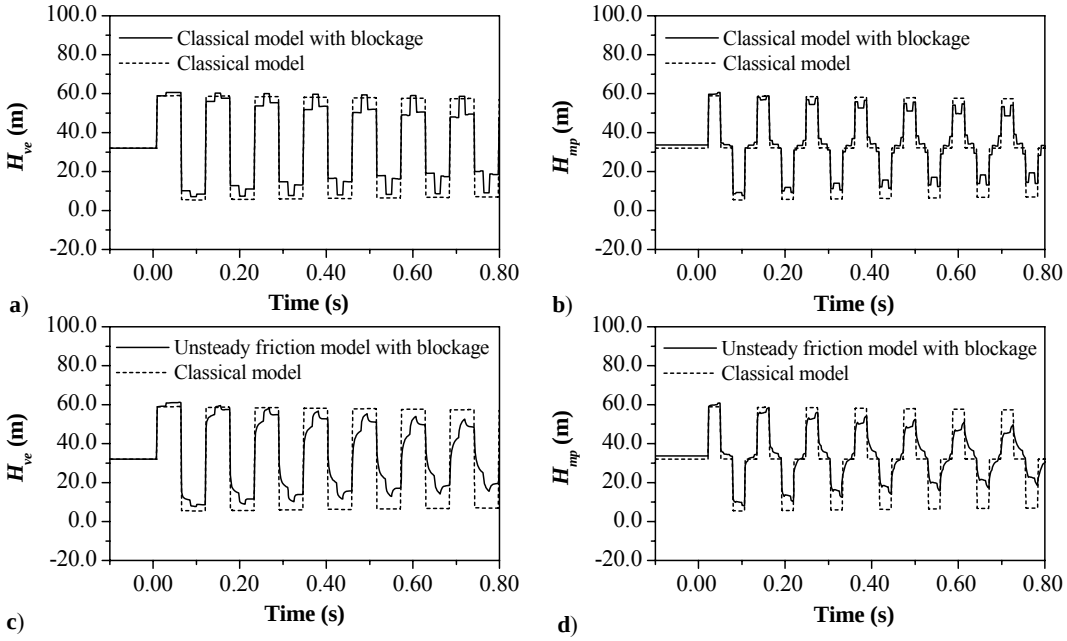

Figure 12 Comparison of heads at the valve (H_{ve}) and at the midpoint (H_{mp}) in a copper pipeline; $\mathbf{Re}_0 = 4{,}360$.

The presence of leaks and blockages creates an attenuation of the pressure response with little dispersion. In this respect their effect is to damp and complicate the pressure response without significantly altering the phase of the response. The addition of unsteady friction in both cases accelerates the attenuation, making the leak- and blockage-induced pressure response shapes less defined. In both cases the leak and blockage contribute largely to the overall damping.

7 Conclusions

The presented case studies clearly show how the effects of unsteady friction, cavitation (including column separation and trapped air pockets), fluid-structure interaction, viscoelastic behaviour of the pipe wall, leakage and blockage change the water-hammer waveform in a simple reservoir-pipeline-valve system. Each case study concerns a classical water-hammer simulation and a corresponding method of characteristics (MOC) numerical model that incorporates each or a combination of the aforementioned effects. The used models are simple and effective and could ideally be combined into one general model. The phenomena studied may cause additional damping (unsteady friction, bubbly flow, fluid-structure interaction in systems with laterally vibrating pipes, viscoelastic behaviour of the pipe-wall, leakage, blockage) or amplification (collapse of large vapour cavities, large trapped gas pockets, fluid-structure interaction) of the

modelled transient traces. A beat phenomenon is predicted for FSI Poisson coupling and for small isolated air pockets. Because the analysed phenomena are not typically modelled in water-hammer software packages, but nevertheless are common in many hydraulic systems, it is important to be able to recognise them. The shown pressure traces can be used as a diagnostic tool for detecting faults and unexpected behaviour in the transient dynamics of liquid-filled pipe systems.

Acknowledgement and disclaimer

The Surge-Net project (see http://www.surge-net.info) is supported by funding under the European Commission's Fifth Framework 'Growth' Programme via Thematic Network "Surge-Net" contract reference: G1RT-CT-2002-05069. The authors of this paper are solely responsible for the content and it does not represent the opinion of the Commission. The Commission is not responsible for any use that might be made of data therein.

Appendix I - References

[1] Bergant A., and Simpson, A.R. (1999). Pipeline column separation flow regimes. *Journal of Hydraulic Engineering*, ASCE, 125(8), 835 - 848.

[2] Bergant, A., Simpson, A.R., and Vítkovský, J.P. (2001). Developments in unsteady pipe flow friction modelling. *Journal of Hydraulic Research*, IAHR, 39(3), 249 - 257.

[3] Bergant, A., and Tijsseling, A.S. (2001). Parameters affecting water hammer wave attenuation, shape and timing. *Proceedings of the 10th International Meeting of the IAHR Work Group on the Behaviour of Hydraulic Machinery under Steady Oscillatory Conditions,* Trondheim, Norway, Paper C2, 12 pp.

[4] Bergant, A., Tijsseling, A.S., Vítkovský, J.P., Covas, D., Simpson, A.R., and Lambert, M.F. (2003). Further investigation of parameters affecting water hammer wave attenuation, shape and timing – Part 1: Mathematical tools and Part 2: Case studies, *Proceedings of the 11th International Meeting of the IAHR Work Group on the Behaviour of Hydraulic Machinery under Steady Oscillatory Conditions,* Stuttgart, Germany, Part 1: 12 pp. and Part 2: 11 pp.

[5] Budny, D.D., Wiggert, D.C., and Hatfield, F.J. (1991). The influence of structural damping on internal pressure during a transient flow. *Journal of Fluids Engineering*, ASME, 113(3), 424 - 429.

[6] Covas, D., Stoianov, I., Mano, J.F., Ramos, H., Graham, N., and Maksimović, Č. (2004, 2005). The dynamic effect of pipe-wall viscoelasticity in hydraulic transients. Part I - experimental analysis and creep characterisation and Part II - model development, calibration and verification. *Journal of Hydraulic Research*, IAHR, Part - I, 42(5), 516 - 530 and Part - II, 43(1), 56 - 70.

[7] Erath, W., Nowotny, B., and Maetz, J. (1999). Modelling the fluid structure interaction produced by a waterhammer during shutdown of high-pressure pumps. *Nuclear Engineering and Design*, 193(3), 283 - 296.

[8] Gally, M., Güney, M., and Rieutord, E. (1979). An investigation of pressure transients in viscoelastic pipes." *Journal of Fluids Engineering*, ASME, 101(4), 495 - 499.

[9] Simpson, A.R., and Bergant, A. (1994). Numerical comparison of pipe-column-separation models. *Journal of Hydraulic Engineering*, ASCE, 120(3), 361 - 377.

[10] Tijsseling, A.S., and Lavooij, C.S.W. (1989). Fluid-structure interaction and column separation in a straight elastic pipe. *Proceedings of the 6th International Conference on Pressure Surges*, BHRA, Cambridge, UK, 27 - 41.

[11] Tijsseling, A.S. (1993). Fluid-structure interaction in case of waterhammer with cavitation. Ph.D. Thesis, Delft University of Technology, Faculty of Civil Engineering, Delft, The Netherlands. Available from: www.darenet.nl/en/page/language.view/search.page.

[12] Tijsseling, A.S., Vardy, A.E., and Fan D. (1996). Fluid-structure interaction and cavitation in a single-elbow pipe system. *Journal of Fluids and Structures*, 10(4), 395 - 420.

[13] Tijsseling, A.S. (1997). Poisson-coupling beat in extended waterhammer theory. *Proceedings of the 4th International Symposium on Fluid-Structure Interactions, Aeroelasticity, Flow-Induced Vibration and Noise*, Dallas, USA, ASME - AD, Vol. 53-2, 529 - 532.

[14] Vardy, A.E., Fan, D., and Tijsseling, A.S. (1996). Fluid/structure interaction in a T-piece pipe. *Journal of Fluids and Structures*, 10(7), 763 - 786.

[15] Vardy, A.E., and Brown, J.M.B. (2003). Transient turbulent friction in smooth pipe flows. *Journal of Sound and Vibration*, 259(5), 1011 - 1036.

[16] Vennatrø, R. (1999). Measurement of velocity profiles in waterhammer and steady oscillatory flow in a rigid steel pipe. *Proceedings of the 9th International Meeting of the IAHR Work Group on the Behaviour of Hydraulic Machinery under Steady Oscillatory Conditions*, Brno, Czech Republic, Paper C5.

[17] Vítkovský, J.P. (2001). Inverse analysis and modelling of unsteady pipe flow: theory, applications, and experimental verification. Ph.D. Thesis, Department of Civil & Environmental Engineering, Adelaide University, Adelaide, Australia.

[18] Vítkovský, J.P., Bergant, A., Simpson, A.R. and Lambert, M.F. (2006). Systematic evaluation of one-dimensional unsteady friction models in simple pipelines. *Journal of Hydraulic Engineering*, ASCE, 132(7), 696 - 708.

[19] Wang, X.J. (2002). Leakage and blockage detection in pipelines and pipe networks. Ph.D. Thesis, Department of Civil & Environmental Engineering, Adelaide University, Adelaide, Australia.

[20] Wylie, E.B. (1984). Simulation of vaporous and gaseous cavitation. *Journal of Fluids Engineering*, ASME, 106(3), 307 - 311.

[21] Wylie, E.B., and Streeter, V.L. (1993). *Fluid Transients in Systems*. Prentice Hall, Englewood Cliffs, USA.

[22] Zielke, W. (1968). Frequency-dependent friction in transient pipe flow. *Journal of Basic Engineering*, ASME, 90(1), 109 - 115.

Appendix II - Notation

The following symbols are used in this paper:

A_{Or} = cross-sectional orifice area;

a = (elastic) liquid wave speed;

a_s = solid wave speed;

$\tilde{a}$ = FSI-modified wave speed (pressure, stress);

C_d = orifice discharge coefficient;

D = internal pipe diameter;

E = Young's modulus of elasticity of pipe-wall material;

e = pipe-wall thickness;

H = piezometric head;

H_{T2} = static head in tank 2 (Fig. 1);

J = creep-compliance function;

J_k = Kelvin-Voigt model parameter;

L = pipe length;

N = number of reaches;

Q = discharge;

$\mathbf{Re}$ = Reynolds number ($\mathbf{Re} = VD/\nu$);

t = time;

t_c = valve closure time;

V = cross-sectionally averaged flow velocity;

W = weighting function for convolution-based unsteady friction model;

α = parameter dependent on the axial pipe constraints;

α_g = gas void fraction;

$\Delta h_{T2\rightarrow T1}$ = pressure head difference between tanks (Fig. 1);

Δt = MOC time step;

Δx = MOC space step;

ν = kinematic viscosity; Poisson's ratio;

ρ_s = mass density of the pipe-wall material;

τ_k = retardation time in Kelvin-Voigt model;

ψ = weighting factor.

Subscripts:

app = approximate;

max = maximum;

mp = midpoint;

Or = orifice;

s = structure, solid, pipe;

ve = valve;

0 = steady-state (initial) conditions;

Abbreviations:

DGCM = discrete gas cavity model;

DVCM = discrete vapour cavity model;

FSI = fluid-structure interaction;

MOC = method of characteristics.